Nanoporous polymeric transmission gratings for high-speed humidity sensing

Jinjie Shi, Vincent K S Hsiao and Tony Jun Huang

Department of Engineering Science and Mechanics, The Pennsylvania State University,
University Park, PA 16802, USA

E-mail: junhuang@psu.edu

Abstract

Nanoporous polymeric transmission gratings are demonstrated to be an excellent platform for high-speed optical humidity sensing. The grating structures were fabricated with a modified holographic, polymer-dispersed liquid crystal (H-PDLC) system. The sensing mechanism was based on changes in the relative transmission associated with the adsorption and desorption of water vapour by nanopores. The spectral changes due to varying humidity levels were measured by a spectrometer and compared with the calculated results based on the coupled wave theory. When the relative humidity (RH) changed from 40% to 95%, the relative transmission at 475 nm increased from 6.3% to 46.6% and that at 702 nm increased from 4% to 64%; these results indicate the sensor's high sensitivity. In addition, the sensor demonstrated excellent reversibility and reproducibility over a large RH range (from 20% to 100% RH). Moreover, the response time of the sensor was measured to be less than 350 ms, making it suitable for many high-speed humidity-sensing applications.

1. Introduction

The measurement of humidity is important for numerous applications such as nuclear power reactors, pulmonary function diagnostics, and residential air conditioners [1–3]. In recent decades, researchers have developed humidity-sensing architectures that use changes in resistance, capacitance, or refractive index (RI) as sensing mechanisms [4–7]. The most widely used humidity-sensing materials include porous ceramics (e.g., Al_2O_3, and TiO_2) [8–14], polymers (such as polyimide and phthalocyanine) [15–24], and polyelectrolytes (e.g., sulfonated polysulfone, polyvinyl acetate) [25–27].

An ideal humidity sensor should have the following characteristics: high sensitivity, broad range of operation, durability, reproducibility, high speed, and low cost [1, 2, 4]. One parameter of particular importance is the time required to respond to changes in relative humidity. A response time on the order of several seconds is considered high speed with current technology [28, 29]. However, humidity sensors with a sub-second response time will be crucial for numerous applications including industrial process controls, monitoring of atmospheric relative humidity (RH), management of patients undergoing anaesthesia, and pulmonary function diagnostics [30, 31].

In this paper, we report the design, fabrication, and characterization of a high-speed optical humidity sensor that is based on nanoporous polymeric transmission gratings. The gratings are fabricated through a modified holographic, polymer-dispersed liquid crystal (H-PDLC) system [32, 33]. This technique involves holographic interference patterning upon a traditional photopolymer mixed with a non-reactive solvent, making possible the rapid fabrication of transmission gratings of varying dimensions. The gratings diffract light upon RI modulation between the porous and nonporous regions. When the RH changes, the RI of the porous regions changes, resulting in increased or decreased intensity of transmitted light. The response time of the sensor was measured to be less than 350 ms. Besides high speed, the nonporous polymer-based humidity sensor demonstrated excellent performance in many categories including sensitivity, range of operation, durability, reproducibility, and cost.

2. Experimental details

The gratings were fabricated by a holographic photopolymerization process [34–36]. First, a pre-polymer syrup was mixed homogenously and sonicated through an analog vortex
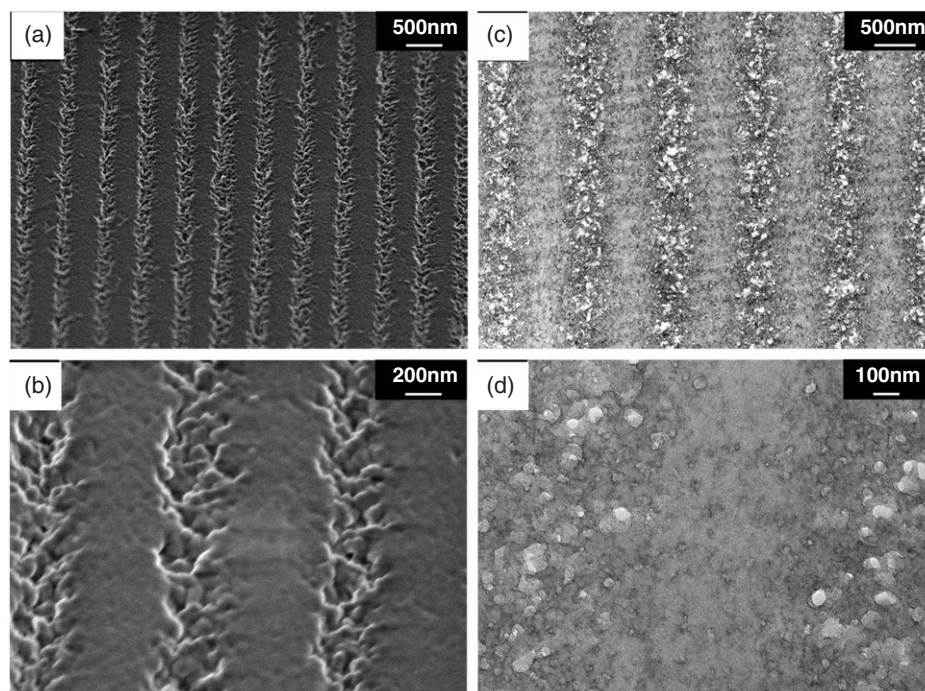
Figure 1. Morphology of nanoporous polymer gratings. (a) and (b) show the surface morphology as characterized by SEM; (c) and (d) show the cross-sectional morphology as characterized by TEM. The bright regions on the TEM images are air voids.

mixer (VWR). The final composition of the pre-polymer syrup contained 10 wt% 3-aminopropyltriethoxysilane (APTES, Aldrich), 25 wt% acetone solution (Aldrich), 15 wt% TL213 liquid crystal (Merck), 40 wt% dipentaerythritol hydroxypenta acrylate (Aldrich), 1 wt% Rose Bengal (Spectra Group Limited), 2 wt% *N*-phenylglycine (Aldrich), and 7 wt% *N*-vinylpyrrolidinone (Aldrich). Second, 20 μl of syrup was placed on a glass slide and covered with a second glass slide that was coated with a non-reactive, 100 nm thick gold layer. The distance between the two glass slides was precisely controlled by adding microbeads (3 μm in diameter) at the edge of the syrup, thereby defining the thickness of the transmission grating. Third, a 514 nm argon ion laser was used to conduct holographic interferometry. In this step, the sandwiched sample was exposed to two 100 mW laser beams at a writing angle of 30° for 1 min. Fourth, immediately following the interference patterning, the sandwiched sample was post-cured under a white light source for 24 h. Finally, due to the poor adhesion between the polymer sample and the gold surface, the sample situated on the bare glass slide was easily separated from the gold-coated cover slide after the post-curing process.

The addition of a non-reactive solvent (such as acetone or toluene) into the pre-polymer syrup is key to the formation of nanopores in the grating. During the photopolymerization process, the solvent phase separated from the photopolymer to form nanoscale droplets. After the droplets of solvent evaporated, nanoscale air voids were left in the polymer structure, forming nanoporous gratings. The addition of APTES greatly improved the adhesion of the structure onto the glass substrate. Figure 1 depicts the surface and cross-sectional morphology of a holographically fabricated, nanoporous polymeric grating, as characterized by low-voltage scanning electron microscopy (SEM) and bright-

field transmission electron microscopy (TEM). The grating was comprised of cross-linked polymer areas (nonporous regions) and periodically alternating, nanoporous polymer areas (porous regions) consisting of nanopores and granular polymer. The precise control of the syrup composition allowed reproduction of the grating spacing, porosity, and thickness. The deviation in diffraction efficiency for most samples from the same batch was generally smaller than 1%. The diameter of the pores ranged from 20 to 100 nm, and could be tuned by changing the composition and concentration of the pre-polymer syrup (e.g., the liquid crystal and non-reactive solvent).

The schematic of the optical measurement setup for humidity sensing is shown in figure 2. A grating was attached to a Teflon substrate of variable angle, and an optical fibre guided light from a halogen lamp to the sample surface. The inset of figure 2 is a side view of the grating structure (the incident angle $\theta = 9°$). The transmitted optical signal was measured by a spectrometer (Ocean Optics Co., HR4000) for a spectral range of 400–1000 nm. A humidity chamber (ESPEC North America Inc., SH-241) integrated with a water tank and a fan system was used to control the operating temperature and humidity. The RH inside the humidity chamber could be programmed and adjusted to any value between 40% and 95%. However, since the chamber required almost 15 min to adjust humidity, a smaller quartz chamber (4 cm × 4 cm × 4 cm) was used to characterize the sensor's response time as the RH was switched between 20% and 100%. The 100% RH was generated by directing a water-vapour-saturated N_2 stream (0.3 l s^{-1}, 20 °C, ~100% RH) into the quartz chamber through a computer-controlled valve [14], while the 20% RH was from the ambient air.
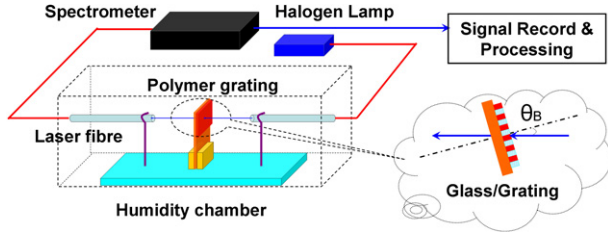
Figure 2. Schematic of the humidity-sensing measurement setup. (This figure is in colour only in the electronic version)

3. Results and discussion

Figure 3(a) shows the spectral response of the grating to different RHs at a constant temperature (34 °C). Each transmission spectrum exhibits two troughs. At 40% RH, the central frequency for the first trough (λ_{trough1}) is at 475 nm and that for the second (λ_{trough2}) is at 702 nm. As the RH increases from 40% to 95%, the positions for both troughs blueshift ($\Delta\lambda_1 = -39$ nm and $\Delta\lambda_2 = -38$ nm). The existence of the two troughs on the transmission spectra and the blueshift of the trough positions can be explained by the coupled wave theory [37]. According to the theory, the diffraction efficiency $\eta_{p(s)}$ and the relative transmission (RT) can be calculated from the following equations:

$$\eta_{p(s)} = \frac{\sin^2[(\nu_{p(s)}^2 + \xi^2)]^{1/2}}{1 + \xi^2/\nu_{p(s)}^2} \tag{1}$$

$$RT = 1 - \eta_{\text{eff}}, \tag{2}$$

where ν and ξ are the modulation and detuning parameters, defined as

$$\nu_p = \frac{\pi n_1 d}{\lambda \cos\theta} \tag{3}$$

$$\nu_s = \nu_p \cos 2\theta \tag{4}$$

$$\xi = \frac{(\theta - \theta_B) K d \cos\theta_B}{2\cos\theta} \tag{5}$$

where θ is the incident angle; θ_B is the Bragg angle; n_1 is the RI modulation; d is the grating thickness; and K is the grating constant. θ_B and K are defined as

$$\theta_B = \sin^{-1}\left(\frac{\lambda}{2\Lambda}\right) \tag{6}$$

$$K = 2\pi/\Lambda, \tag{7}$$

where λ is the wavelength of incident light and Λ is the grating spacing [38]. Since non-polarized incident light was used in the experiment, the average diffraction efficiency η_{eff} [38] was employed in the calculation. For the grating used in the experiments, $\Lambda = 830$ nm; $\theta = 9°$; $\theta_B = 36°$; $d = 3.2$ μm; $porosity = 10\%$; $n_{\text{polymer}} = 1.52$; $n_{\text{air}} = 1.005$ (at 40% RH); and $n_{\text{water vapour}} = 1.043$ (at 100% RH) [15, 39]. Using these parameters in equations (2)–(7), the relative transmission was found as a function of λ (figure 3(b)). Similar to the experimental results (figure 3(a)), two troughs were observed on the theoretical transmission curve from 400 to 900 nm. The calculated trough positions (located at $\lambda_1 = 470$ nm and $\lambda_2 = 705$ nm for 40% RH, figure 3(b)) match well with the
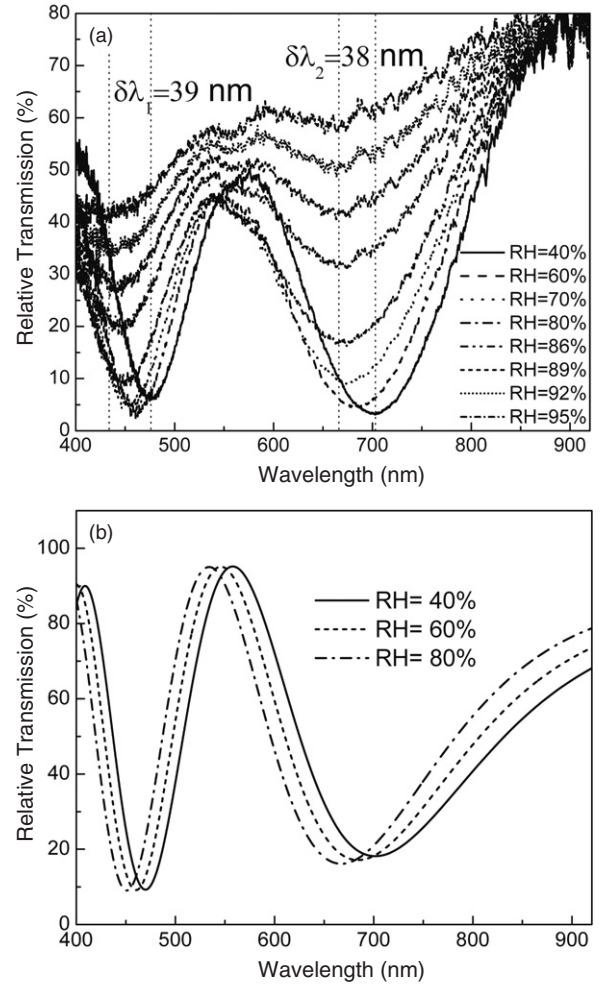

Figure 3. (a) The transmission spectra of a typical grating at various RH, recorded by a spectrometer. The relative transmission is the ratio of the transmitted signal to the normalized incident light. (b) The calculated transmission spectrum based on the coupled wave theory (40%, 60% and 80% RH).

experimental results ($\lambda_1 = 475$ nm and $\lambda_2 = 702$ nm for 40% RH, figure 3(a)). However, a comparison of figures 3(a) and (b) also shows that there is a discrepancy between the calculated RT and the experimental value. This discrepancy is mainly because the light absorbance, reflection, and RI mismatch between the grating structure and the glass substrate were not considered in our model. Despite these drawbacks, our model can predict the existence and exact positions of the two troughs at various RH (figure 3(b)).

Figure 3(a) shows that, when the RH increases, the positions for both troughs blueshift and the transmission intensity at the second trough increases. Both behaviours are caused by variations in the RI contrast between the porous and nonporous regions of the grating. Higher humidity leads to smaller RI contrast and thus lower diffraction efficiency and greater transmission intensity. Figure 3(a) also shows that when the RH increases from 40% to 60%, there is a slight drop (3%) in the transmission intensity at the central wavelength for the first trough. This phenomenon was likely caused by the increased light absorbance in the polymeric grating structure. As the RH continued to increase, the transmission intensity at
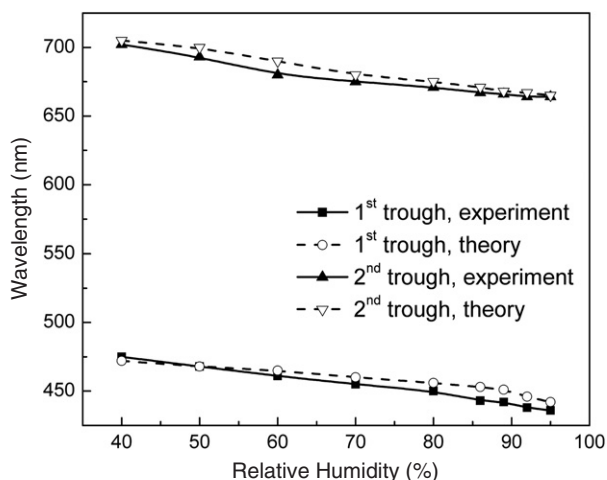
Figure 4. Experimental and theoretical results for the two trough positions as a function of RH.

Figure 5. Relative transmission as a function of RH at two characteristic wavelengths (475 and 702 nm).

the first trough started to increase, because of the decreasing RI contrast between the porous and nonporous regions.

Figure 4 plots the experimental and theoretical trough positions (for both troughs) as a function of RH. The plot shows that the experimental and theoretical results match well. The RI of the nanopores at various RH levels was calculated based on a linear extension of n_{air} (40% RH) and $n_{water\ vapour}$ (100% RH). The excellent matching of the trough positions between the experimental and theoretical results indicate that the physical parameters for the polymeric gratings (e.g., grating spacing, thickness) remained unchanged during the adsorption/desorption process. On the other hand, the results for the organic vapour sensing application [36] showed that severe polymer swelling occurred as organic vapour such as acetone and methanol adsorbed in the nanoporous polymeric structures. The contrasts between our humidity-sensing result and the organic vapour-sensing one indicate that the nanoporous polymeric grating-based humidity sensor has excellent selectivity over organic vapour.

As observed from figure 3(a), the transmission intensity for any wavelength located in the right portion of both troughs (470–530 nm for the first trough and 705–800 nm for the second) increases with increasing RH. At the central wavelengths of the troughs, the maximum changes of the transmission intensity and thus the highest sensitivity can be obtained. Figure 5 depicts the evolution of relative transmission as a function of RH at two characteristic wavelengths (475 and 702 nm). As the RH increases from 40% to 95%, the relative transmission at 475 nm increases from 6.3% to 46.6%, and that at 702 nm increases from 4% to 64%. These large increases indicate that high sensitivity can be achieved at these characteristic wavelengths and that the sensitivity can be tuned by changing the wavelength. Figure 5 also shows that the response curves for both wavelengths are not linear and that the detection sensitivity is higher at the high-humidity region (RH > 80%). However, even at the 'low-sensitivity' region (RH < 60%), the changes in transmission intensity are still large enough ($\Delta RT/\Delta RH = 0.15$ at $\lambda = 475$ nm and $\Delta RT/\Delta RH = 0.25$ at $\lambda = 702$ nm) to be detected by a regular spectrometer, as shown in figure 3.
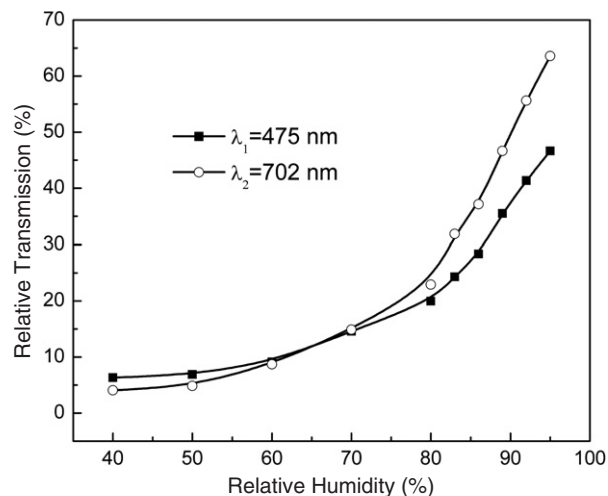
The stability and repeatability of the humidity sensors over a large RH range was further demonstrated in a multi-cycle experiment, where saturated water vapour (100% RH) was periodically introduced into the smaller quartz humidity chamber (20% RH). Figure 6(a) shows that, as the RH periodically oscillated between 20% and 100%, the relative transmission at $\lambda = 700$ nm switched between 3% and 75%. This response is highly reproducible because the difference in relative transmission among more than 100 experimental cycles was less than 1%—figure 6(a) only shows five of the cycles.

Figure 6(b) indicates that the response time of the adsorption process (from 20% to 100% RH) is about 350 ms, and that for the desorption process (from 100% to 20% RH) is about 9 s. The difference in the response time for the adsorption process and desorption is caused by two reasons. First, generally it takes longer for water molecules to diffuse from nanopores to the environment than by the opposite route. Second, during the adsorption process, a fan was employed to bring a water-vapour-saturated N_2 stream to the humidity chamber, while for the desorption process, water vapour diffused naturally from the humidity chamber to the ambient environment, which takes much longer. We must emphasize that the measured value of 350 ms for the adsorption process (or 9 s for the adsorption process) may not be the intrinsic speed of the humidity-sensing polymeric structure. Rather, the value we found is due to two factors: the time needed for vapour to diffuse through the chamber (this process is limited by our experimental setup); and the time needed for the vapour to saturate the nanopores (this process indicates the intrinsic speed of our sensor). Taking into account the size of the chamber (4 cm × 4 cm × 4 cm) and the flow rate ($0.3\ 1\ s^{-1}$) of the water vapour, we concluded that ∼213 ms was needed for vapour to completely displace the volume in the chamber. The intrinsic adsorption time of the grating was thus about 137 ms. If a smaller chamber or higher flow rate were to be used, a smaller time constant would be expected. The response time and sensitivity of the sensor are also dependent upon its porosity. A higher porosity or smaller pore size leads to a
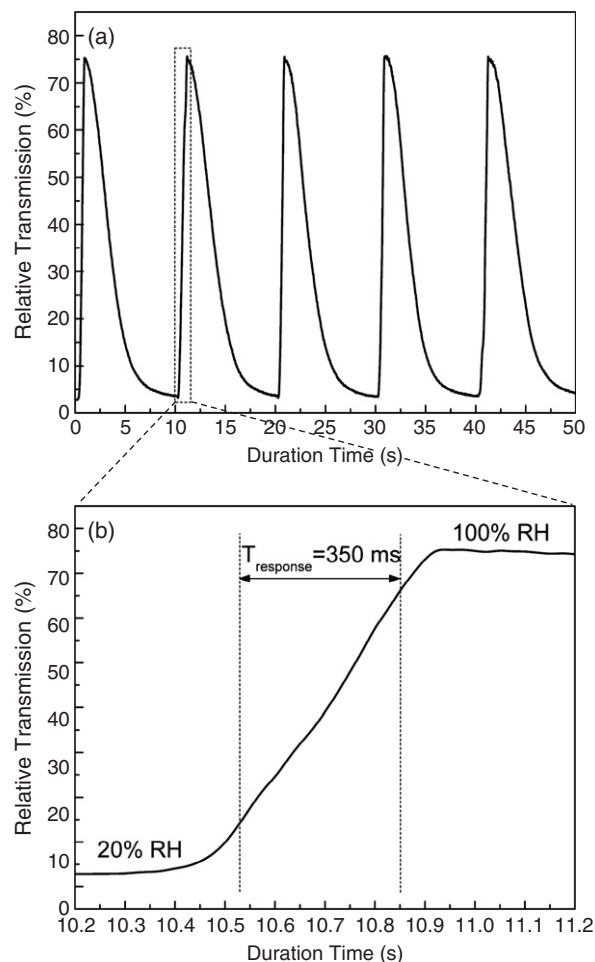
Figure 6. The time-dependent transmission curve ($\lambda = 700$ nm, $T = 20\,°$C) (a) as the RH oscillates between 20% and 100% for multiple cycles, and (b) as the RH increases from 20% to 100%.

larger change in the average RI, thus generating a larger shift in the bandgap and yielding better sensitivity. These changes, however, also cause a longer response time. By optimizing the porosity, film thickness and grating spacing, one can balance requirements for response time and detection sensitivity.

4. Conclusion

In this work, we have presented a nanoporous, polymeric grating-based humidity sensor that features excellent speed, sensitivity, range of operation, durability, and reproducibility. The grating structures were fabricated by a holographic photopolymerization process. Using a model based on the coupled wave theory, we were able to predict the existence and positions of two troughs on the transmission spectra at various relative humidities. However, to quantitatively predict the transmission intensity at various wavelengths and humidities, a more sophisticated model will be needed. The sensitivity of the sensor is dependent on its wavelength. At the central wavelengths of the troughs, the maximum changes of the transmission intensity and thereby the highest sensitivities can be obtained. In addition, the sensor demonstrates excellent reversibility and reproducibility over a large range of RH. Less

than 1% difference in the relative transmission was observed among hundreds of experimental cycles. The intrinsic response time of the sensor is $\sim$137 ms, indicating its potential in numerous high-speed, humidity-sensing applications.

References

[1] Yamazoe N and Shimizu Y 1986 Humidity sensors: principles and applications *Sensors Actuators* **10** 379–98
[2] Fenner R and Zdankiewicz E 2001 Micro-machined water vapor sensors: a review of sensing technologies *IEEE Sensors* **14** 309–17
[3] Huang J R, Li M Q, Huang Z Y and Liu J H 2007 A novel conductive humidity sensor based on field ionization from carbon nanotubes *Sensors Actuators* A **133** 467–71
[4] Chen Z and Lu C 2005 Humidity sensors: a review of materials and mechanisms *Sensors Lett.* **3** 274–95
[5] Kim S J, Park J Y, Lee S H and Yi S H 2000 Humidity sensors using porous silicon layer with mesa structure *J. Phys. D: Appl. Phys.* **33** 1781–4
[6] Okcan B and Akin T 2004 *Proc. 17th IEEE Int. Conf. on Micro Electro Mechanical Systems (Maastricht, 2004)* pp 552–5
[7] Muto S, Osamu S, Takashi A and Masayuki M 2003 A plastic optical fibre sensor for real-time humidity monitoring *Meas. Sci. Technol.* **14** 746–50
[8] Traversa E 1995 Ceramic sensors for humidity detection: the state-of-the-art and future developments *Sensors Actuators* B **23** 135–56
[9] Kulwicki B M 1991 Humidity sensors *J. Am. Ceram. Soc.* **74** 697–708
[10] Kang U and Wise K D 2000 A high-speed capacitive humidity sensor with on-chip thermal reset *IEEE Trans. Electron. Devices* **47** 702–10
[11] Connolly E J, Pham H T M, Groeneweg J, Sarro P M and French P J 2004 Relative humidity sensors using porous SiC membranes and Al electrodes *Sensors Actuators* B **100** 216–20
[12] Seiyama T, Yamazoe N and Arai H 1983 Ceramic humidity sensors *Sensors Actuators* **4** 85–96
[13] Zambov L M, Popov C, Plass M F, Bock A, Jelinek M, Lancok J, Masseli K and Kulisch W 2000 Capacitance humidity sensor with carbon nitride detecting element *Appl. Phys.* A **70** 603–6
[14] Kalkan A K, Li H D, O'Brien C J and Fonash S J 2004 A rapid-response, high-sensitivity nanophase humidity sensor for respiratory monitoring *IEEE Electron Device Lett.* **25** 526–8
[15] Tsigara A, Mountrichas G, Gatsouli K, Nichelatti A, Pispas S, Madamopoulos N, Vainos N A, Du H L and Roubani-Kalantzopoulou F 2007 Hybrid polymer/cobalt chloride humidity sensors based on optical diffraction *Sensors Actuators* B **120** 481–6

[16] Wang J, Shi K, Chen L and Zhang X 2004 Study of polymer humidity sensor array on silicon wafer *J. Mater. Sci.* **39** 3155–7

[17] Zajt T, Jasiñski G and Chachuiski B 2003 Electrical properties of polymer humidity sensor based on polyethyleneimine *Proc. SPIE* **5124** 130–7

[18] Nomura T, Yasuda T and Furukawa S 1993 Humidity sensor using surface acoustic waves propagating along polymer/LiNbO$_3$ structures *Ultrasonics Symp.* pp 417–20

[19] Wang J, Wu F Q, Shi K H, Wang X H and Sun P P 2004 Humidity sensitivity of composite material of lanthanum ferrite/polymer quaternary acrylic resin *Sensors Actuators* B **99** 586–91

[20] Sakai Y, Matuguchi M, Sadaoka Y and Hirayama K 1993 A humidity sensor composed of interpenetrating polymer networks of hydrophilic and hydrophobic methacrylate polymers *J. Electrochem. Soc.* **140** 432–6

[21] Nomura T, Oofuchi K, Yasuda T and Furukawa S 1994 SAW humidity sensor using dielectric hygroscopic polymer film *Ultrasonics Symp.* pp 503–6

[22] Yang B, Aksak B, Lin Q and Sitti M 2006 Compliant and low-cost humidity sensors using nano-porous polymer membranes *Sensors Actuators* B **114** 254–62

[23] Yao Z and Yang M 2006 A fast response resistance-type humidity sensor based on organic silicon containing cross-linked copolymer *Sensors Actuators* B **117** 93–8

[24] Albrecht B A, Benson C H and Beuermann S 2003 Polymer capacitance sensors for measuring soil gas humidity in drier soils *Geotech. Test. J.* **26** 3–11

[25] Rubinger C P L, Martins C R, De Paoli M A and Rubinger R M 2007 Sulfonated polystyrene polymer humidity sensor: synthesis and characterization *Sensors Actuators* B **123** 42–9

[26] Steele J J, van Popta A C, Hawkeye M M, Sit J C and Brett M J 2006 Nanostructured gradient index optical filter for high-speed humidity sensing *Sensors Actuators* B **120** 213–9

[27] Adhikari B and Majumdar S 2004 Polymers in sensor applications *Prog. Polym. Sci.* **29** 699–766

[28] Connolly E J, O'Halloran G M, Pham H T M, Sarro P M and French P J 2002 Comparison of porous polysilicon and porous silicon carbide as materials for humidity sensing applications *Sensors Actuators* A **99** 25–30

[29] Rittersma Z M, Splinter A, Bödecker A and Benecke W 2000 A novel surface-machined capacitive porous silicon humidity sensor *Sensors Actuators* B **68** 210–7

[30] Laville C and Pellet C 2002 Comparison of three humidity sensors for a pulmonary function diagnosis microsystem *IEEE Sensors J.* **2** 96–101

[31] Tatara T and Tsuzaki K 1997 An apnea monitor using a rapid-response hygrometer *J. Clin. Monit.* **13** 5–9

[32] Matsuoka S, Wallder V T and Beauchamp H L 1971 Application of holographic interference technique to mechanical studies of polymeric solids *Polym. Eng. Sci.* **11** 46–50

[33] Bunning T J, Natarajan L V, Tondiglia V P and Sutherland R L 2000 Holographic polymer-dispersed liquid crystals (H-PDLCS) *Annu. Rev. Mater. Sci.* **30** 83–115

[34] Hsiao V K S, Lin T C, He G S, Cartwright A N and Prasad P N 2005 Optical microfabrication of highly reflective volume Bragg gratings *Appl. Phys. Lett.* **86** 131113

[35] Natarajan L V, Shepherd C K, Brandelik D M, Sutherland R L, Chandra S, Tondiglia V P, Tomlin D and Bunning T J 2003 Switchable holographic polymer-dispersed liquid crystal reflection gratings based on thiol-ene photopolymerization *Chem. Mater.* **15** 2477–84

[36] Hsiao V K S, Kirkey W D, Chen F, Cartwright A N, Prasad P N and Bunning T J 2005 Organic solvent vapor detection using holographic photopolymer reflection gratings *Adv. Mater.* **17** 2211–4

[37] Kogelnik H and Shank C V 1972 Coupled-wave theory of distributed feedback lasers *J. Appl. Phys.* **43** 2327–35

[38] Sheat D E and Miles A J M 1991 *The 3rd Int. Conf. on Holographic Systems, Components, and Applications (Edinburgh, 1991)* pp 83–7

[39] Ciddor P E 1996 Refractive index of air: new equations for the visible and near infrared *Appl. Opt.* **35** 1566–73